J. Math. Computer Sci., 41 (2026), 437–455

Online: ISSN 2008-949X

Journal of Mathematics and Computer Science

Journal Homepage: www.isr-publications.com/jmcs

Efficient computational framework for solving boundary value problems in Caputo setting with polynomial and non-polynomial solutions

Misbah Wajiha[a], Imran Talib[b,*], Dumitru Baleanu[c], Muhammad Sadiq Hashmi[a]

[a]*Department of Mathematics, The Government Sadiq College Women University, Girls College Road, Anwar Colony, Bahawalpur, 63100, Punjab, Pakistan.*

[b]*Nonlinear Analysis Group, Department of Mathematics, Virtual University of Pakistan, 54-Lawrence Road, Lahore, 54000, Punjab, Pakistan.*

[c]*Department of Computer Science and Mathematics, Lebanese American University, Beirut, Lebanon.*

Abstract

In the presented study, we address two-point boundary value problems in the Caputo framework by extending the operational matrices approach. This approach has previously been used in the literature to solve problems modeled with initial conditions. The proposed method relies on newly constructed operational matrices for fractional-order integrals derived from shifted Gegenbauer polynomials. Through the inclusion of monomial terms in the proposed computational scheme, these matrices convert the problem into Sylvester-form matrix equations that can be resolved effectively. Moreover, our approach is applicable to problems admitting either polynomial or non-polynomial solutions. In order to assess the precision and efficiency of our method, we compare its results with those produced by the Bessel Collocation approach, the Haar Wavelet approach, a hybrid approach combining the Homotopy Perturbation approach with Green's function, and the Fractional Central Formula for the Caputo differentiator. This comparative analysis confirms the effectiveness of our approach.

Keywords: Gegenbauer polynomials, operational matrices approach, boundary value problems, Caputo fractional derivative, special functions, orthogonal polynomials, fractional differential equations.

2020 MSC: 26A33, 34A08, 34B05, 65L10.

1. Introduction

Fractional calculus emerged in 1695, shortly after the development of classical calculus, and is closely linked to the dynamics of complex real-world problems. At an early stage of its development, it was long considered purely theoretical. Fractional calculus is rapidly advancing today, with convincing applications across multiple fields including bioengineering [21, 22], neuroscience [5, 6], and computer science [13, 24].

*Corresponding author

Email addresses: smisbah104@gmail.com (Misbah Wajiha), imrantaalib@gmail.com, imrantalib@vu.edu.pk (Imran Talib), dumitru.baleanu@lau.edu.lb (Dumitru Baleanu), sadiq.hashmi@gmail.com (Muhammad Sadiq Hashmi)

doi: 10.22436/jmcs.041.04.01

Received: 2024-11-28 *Revised:* 2025-08-14 *Accepted:* 2025-09-18

To solve fractional order differential equations (FODEs), operational matrix approaches using orthogonal polynomials have been broadly implemented in numerical methods, as discussed in [7, 18, 30, 31, 37, 38]. These methods transform the derivative terms in the equations into derivative operational matrices. By this transformation, the problem reduces to a set of simple algebraic equations, which can be easily solved using computational software, and their solution provides the result of the original FODEs. However, the results presented in [7, 18, 30, 31, 38] are limited to addressing problems with initial conditions. Therefore, this study aims to address the following problem with two-point boundary conditions (TPBCs):

$$ {}_C\mathcal{D}^{\alpha_0}Y(x) = a_1\,{}_C\mathcal{D}^{\beta_0}Y(x) + a_2Y(x) + F(x), \quad x \in [0,1], \quad Y(0) = p_0, \quad Y(1) = p_1, \tag{1.1} $$

Here, ${}_C\mathcal{D}$ denotes the Caputo fractional order derivative, where $0 < \beta_0 < \alpha_0 \leqslant 2$. Here, a_1, a_2, p_0, and p_1 are representing the real constant. $F(x)$ represents a source term, and the problem's solution (1.1) is expressed by the function $Y(x)$.

The problem (1.1) has been previously addressed in [36] using the Bessel Collocation Method (BCM) with $\alpha_0 = 2$ and $\beta_0 = 1.5$. Similarly, in [33], the authors employed the Haar Wavelet Method (HWM) to solve (1.1) with $\alpha_0 = 2$ and $\beta_0 = 1.5$. The problem was also studied in [35] through the Homotopy Perturbation Method with Green's function (HPGF), considering $\alpha_0 = 2$ and $\beta_0 = 1$. Additionally, [2] employed the Fractional Finite Difference Method (FFDM) to solve (1.1). Further investigations using the Pseudo-Spectral Method (PSM) and the Generalized Adams-Bashforth-Moulton Method (GABMM) are reported in [9, 12], where $\alpha_0 = 1.5$ was considered. Recently, [4] proposed the Fractional Central Formula for the Caputo Differentiator (FCFCD) for solving (1.1) with $0 < \alpha_0 \leqslant 1$. For further exploration of boundary value problems covering various types of boundary conditions, we refer readers to [11, 16, 19, 20]. Recent work by [17] introduced a computational approach to handle nonlinear FODEs of multiple orders, employing Caputo derivatives and operational matrices of Hosoya polynomials.

Inspired by insights from the literature and the broad applicability of boundary value problems across various scientific disciplines such as astrodynamics, physics, and epidemiology [8, 14, 27], we address problem (1.1) using distinct methodologies, diverging from those discussed in [2, 4, 33, 35, 36]. Furthermore, we extend previous findings discussed in [7, 18, 30, 31, 38], which were developed for solving problem (1.1) with initial conditions. Now, we extend these methodologies to solve problem (1.1) involving TPBCs. This transformation is carried out by embedding monomial terms into the algorithm, facilitated through the construction of new integral matrices for fractional-order operators within the framework of shifted Gegenbauer polynomials (GPs). By enabling the incorporation of monomial terms, these matrices reformulate problem (1.1) into matrix equations of the Sylvester form, which can be handled with relative ease. In contrast, the algorithms proposed in [7, 18, 30, 31, 38] do not support the integration of monomial terms for solving problem (1.1). Additionally, our proposed method (PM) is well fit to solve the problems with polynomial as well as non-polynomial solutions.

To demonstrate the effectiveness of our PM, we conduct a comprehensive numerical comparison with existing methods such as BCM [36], HWM [33], HPGF [35], PSM [12], GABMM [9], and FCFCD [4]. Our findings indicate that PM achieves higher computational efficiency and versatility in handling polynomial as well as non-polynomial solutions.

The structure of this article is as follows. Section 2 introduces the basic concepts and key characteristics of fractional-order operators that are necessary for the later analysis. Section 3 provides necessary details on GPs, including their analytical expressions and properties. Section 4 outline fractional-order integral and derivative operational matrices of GPs. Additionally, this section introduces a new definite integral operational matrix, representing a central contribution of our study. Section 5 discusses the development of the PM for solving FODEs with TPBCs. Section 6 covers the error analysis part of the manuscript. In Section 7, we present various examples demonstrating the effectiveness of the PM compared to existing methods. Finally, the paper concludes in Section 8 with a summary of our investigation, key findings, and future directions.

2. Fractional calculus

This section outlines some essential properties and fundamental definitions of fractional-order operators that will be referenced throughout this article. Although the literature presents various definitions for fractional-order integrals and derivatives, they are not equivalent. The most commonly used definitions are those of Riemann-Liouville and Caputo, as explained below.

Definition 2.1 ([26]). . The Riemann-Liouville fractional-order integral provides a generalization of the classical integral to fractional orders and is expressed as:

$$ {}_{RL}I^{\gamma}_{g^+}\nu(x) = \frac{1}{\Gamma(\gamma)}\int_g^x (x-\eta)^{\gamma-1}\nu(\eta)d\eta, \quad x > g, \quad \gamma \in \mathbb{R}_+. $$

Thus, the definitions of fractional-order derivative operators in both the Riemann-Liouville and Caputo frameworks are given by:

$$ {}_{RL}\mathcal{D}^{\gamma}_{g^+}\nu(x) = D^p_{RL}I^{p-\gamma}_{g^+}\nu(x) = \frac{1}{\Gamma(p-\gamma)}\frac{d^p}{dx^p}\int_g^x (x-\eta)^{p-\gamma-1}\nu(\eta)\,d\eta, \quad x > g, $$
$$ {}_{C}\mathcal{D}^{\gamma}_{g^+}\nu(x) = {}_{RL}I^{p-\gamma}_{g^+}D^p\nu(x) = \frac{1}{\Gamma(p-\gamma)}\int_g^x (x-\eta)^{p-\gamma-1}\nu^{(p)}(\eta)\,d\eta, \quad x > g. $$

The symbols ${}_{RL}\mathcal{D}$ and ${}_{C}\mathcal{D}$ represent the fractional-order derivative operators in the Riemann-Liouville and Caputo frameworks, respectively, where the order satisfies $p-1 < \gamma < p$, $p \in \mathbb{N}$. The following properties will be useful for establishing the main results later [26]:

$$ {}_{RL}I^{\gamma}_{g^+}(x-g)^q = \frac{\Gamma(q+1)}{\Gamma(q+1+\gamma)}(x-g)^{q+\gamma}, \ \gamma \in \mathbb{R}_+, $$
$$ {}_{C}\mathcal{D}^{\gamma}_{g^+}(x-g)^q = \frac{\Gamma(q+1)}{\Gamma(q+1-\gamma)}(x-g)^{q-\gamma}, \ q \in \mathbb{R}_+, \ q \geqslant \lceil\gamma\rceil, \tag{2.1} $$
$$ {}_{C}\mathcal{D}^{\gamma}_{g^+}(u(x)+\nu(x)) = {}_{C}\mathcal{D}^{\gamma}_{g^+}u(x) + {}_{C}\mathcal{D}^{\gamma}_{g^+}\nu(x). \tag{2.2} $$

3. Shifted GPs [1]

Gegenbauer polynomials, also known as ultraspherical polynomials, have significant applications across various scientific disciplines due to their unique properties and orthogonality relations. These polynomials feature a weight function of broader generality and are defined over the interval $[-1,1]$. The Legendre and Chebyshev polynomials are the special case of these polynomials (see [1]). GPs naturally arise as extensions of Legendre polynomials within the domains of potential theory and harmonic analysis. Additionally, they are found in the theory of positive-definite functions, for detail see [28]. They are particularly important in the study of quantum mechanics in many-body systems, as they provide a natural method for expanding certain functions. For more information, see sources [23, 29].

The GPs $O^{\beta}_i(x)$ defined on the interval $[-1,1]$ have the following explicit formula:

$$ O^{\beta}_i(x) = \sum_{p=0}^{\lfloor \frac{i}{2} \rfloor} \frac{(-1)^p\Gamma(i-p+2\beta)}{p!\Gamma(\beta)(i-2p)!}2x^{i-2p}. \tag{3.1} $$

For applying these polynomials over the interval $[0,1]$, the shifted GPs are constructed by introducing the transformation $x = 2t-1$, as described in [34],

$$ G^{\mu}_e(x) = \frac{\Gamma(\mu+\frac{1}{2})}{\Gamma(2\mu)}\sum_{p=0}^{e}\frac{(-1)^{e-p}\Gamma(e+p+2\mu)}{\Gamma(p+\mu+\frac{1}{2})(e-p)!p!}x^p. \tag{3.2} $$

The shifted GPs $G_e^{\mu}(x)$, introduced in Eq. (3.2), are orthogonal on the interval $[0,1]$ with respect to the weight function $w(x) = (x(1-x))^{\mu-\frac{1}{2}}$. The corresponding orthogonality relation is given by:

$$\int_0^1 G_e^{\mu}(x) G_b^{\mu}(x) w(x) dx = \begin{cases} 0, & \text{for } e \neq b, \\ y_b, & \text{for } e = b, \end{cases}$$

where, $y_b = \frac{\Gamma(\mu+\frac{1}{2})^2 \Gamma(b+2\mu)}{\Gamma(2\mu)^2 (2b+2\mu) b!}$. By using Eq. (3.2), we can calculate the first few shifted GPs for $e = 0, 1, \cdots, 4$ and $\mu = 1$, as shown below:

$$\begin{pmatrix} G_0^1(x) \\ G_1^1(x) \\ G_2^1(x) \\ G_3^1(x) \\ G_4^1(x) \end{pmatrix} = \begin{pmatrix} 1 \\ 4x-2 \\ 16x^2-16x+3 \\ 64x^3-96x^2+40x-4 \\ 256x^4-512x^3+336x^2-80x+5 \end{pmatrix}.$$

3.1. Function approximation using Gegenbauer series

An arbitrary function $v \in L^2([0,1]; (x-x^2)^{\mu-\frac{1}{2}})$, having finite integral

$$\|v\|^2 = \int_0^1 (x-x^2)^{\mu-\frac{1}{2}} |v(x)|^2 dx < \infty$$

can be represented as an expansion in the shifted Gegenbauer series:

$$v(x) = \lim_{n \to M-1} \sum_{e=0}^{n} a_e G_e^{\mu}(x). \tag{3.3}$$

The coefficients of the series in Eq. (3.3) can be computed using the following expression:

$$a_e = \int_0^1 v(x) (x-x^2)^{\mu-\frac{1}{2}} G_e^{\mu}(x) dx. \tag{3.4}$$

By truncating the series to its first $M-1$ terms, Eq. (3.3) can be rewritten as follows:

$$v(x) \approx \sum_{e=0}^{M-1} a_e G_e^{\mu}(x) = \Theta_{M-1}^T \Lambda_{M-1}(x), \tag{3.5}$$

where,

$$\Theta_{M-1}^T = [a_0, a_1, a_2, \ldots, a_{M-1}], \quad \Lambda_{M-1}(x) = \left[G_0^{\mu}(x), G_1^{\mu}(x), \ldots, G_{(M-1)}^{\mu}(x)\right]^T.$$

Let's examine a quartic function $v(x) = \frac{x^4}{3} + 2x^3$ that possesses a finite square norm under the weight $(x-x^2)^{\mu-\frac{1}{2}}$, where $\mu = 1$:

$$\left\| \frac{x^4}{3} + 2x^3 \right\|^2 = \int_0^1 \left(\frac{x^4}{3} + 2x^3 \right)^2 (x-x^2)^{\mu-\frac{1}{2}} dx = 0.213.$$

Thus, the function $(\frac{x^4}{3} + 2x^3) \in L^2\left([0,1]; (x-x^2)^{\mu-\frac{1}{2}}\right)$ can be expanded into shifted Gegenbaeur series, as follows:

$$\frac{x^4}{3} + 2x^3 \approx \sum_{e=0}^{M-1} a_e G_e^{\mu}(x),$$

where the coefficients are given by $a_0 = 0.193$, $a_1 = 0.196$, $a_2 = 0.087$, $a_3 = 0.016$, $a_4 = 0.000511$. Therefore,

$$\frac{x^4}{3} + 2x^3 \approx 0.193G_0^1(x) + 0.196G_1^1(x) + 0.087G_2^1(x) + 0.016G_3^1(x) + 0.0005G_4^1(x).$$

Let's consider another function $v(x) = x\sin(2x) + x^{\frac{1}{2}}$ with $\mu = 1$:

$$\left|\left|x\sin(2x) + x^{\frac{1}{2}}\right|\right|^2 = \int_0^1 (x\sin(2x) + x^{\frac{1}{2}})^2 (x - x^2)^{\mu - \frac{1}{2}} dx = 0.575,$$

where the coefficients are given by $a_0 = 0.436$, $a_1 = 0.187$, $a_2 = -0.008$, $a_3 = -0.0069$, $a_4 = -0.0028$. Thus, we can express $v(x) = x\sin(2x) + x^{\frac{1}{2}}$ into shifted Gegenbaeur series, as follows:

$$x\sin(2x) + x^{\frac{1}{2}} \approx 0.436G_0^1(x) + 0.187G_1^1(x) - 0.008G_2^1(x) - 0.0069G_3^1(x) - 0.0028G_4^1(x).$$

Now, consider the rational function $z(x) = \frac{\frac{x^4}{3}+2x^3}{x^3+1}$ that possesses a finite square norm under the weight $(x - x^2)^{\mu - \frac{1}{2}}$, i.e.,

$$\left|\left|\frac{\frac{x^4}{3} + 2x^3}{x^3 + 1}\right|\right|^2 = \int_0^1 \left(\frac{\frac{x^4}{3} + 2x^3}{x^3 + 1}\right)^2 (x - x^2)^{\mu - \frac{1}{2}} dx = 0.0865.$$

Hence, $\frac{\frac{x^4}{3}+2x^3}{x^2+1} \in L^2([0,1]; (x - x^2)^{\mu - \frac{1}{2}})$ and it can be expanded into shifted Gegenbauer series. The series coefficients are given as $a_0 = 0.37$, $a_1 = 0.406$, $a_2 = 0.250$, $a_3 = 0.149$, $a_4 = 0.117$.

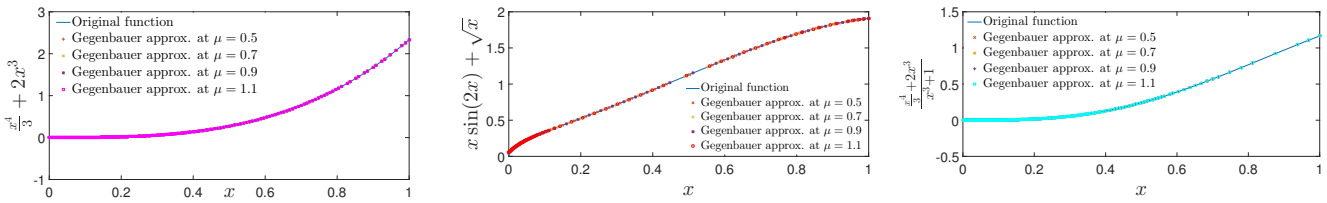

(a) $M = 5$ **(b)** $M = 10$ **(c)** $M = 10$

Figure 1: Gegenbauer approximation for various values of μ.

4. Operational matrices of shifted GPs

Lemma 4.1. *The fractional-order Caputo derivative* ${}_C\mathcal{D}_{0^+}^{\alpha} G_e^{\mu}(x)$ *of* α *order of shifted GPs defined in* (3.2) *can be computed as*

$${}_C\mathcal{D}_{0^+}^{\alpha} G_e^{\mu}(x) = \begin{cases} \frac{\Gamma(\mu+\frac{1}{2})}{\Gamma(2\mu)} \sum_{p=\lceil\alpha\rceil}^{e} \frac{(-1)^{e-p}\Gamma(e+p+2\mu)\Gamma(p+1)}{\Gamma(p+\mu+\frac{1}{2})\Gamma(p+1-\alpha)(e-p)!p!} x^{p-\alpha}, & e = \lceil\alpha\rceil, \ldots, M-1, \\ 0, & e = 0, 1, \ldots, \lceil\alpha\rceil - 1. \end{cases}$$

Proof. Using Eq. (2.1), Eq. (2.2), and Eq. (3.2), the result can be proved. □

4.1. Novel operational matrix in Riemann-Liouville framework of shifted GPs

In various fields of applied mathematics, particularly in computational mathematics, operational matrices associated with orthogonal polynomials play a crucial role in the development of the spectral methods [7, 18, 30, 31, 38]. Matrix operations can be used to describe differential and integral operators by using operational matrices connected to orthogonal polynomials. This makes it possible to convert FODEs into algebraic equations, which significantly simplifies obtaining numerical solutions.

In this section, we discuss the construction of a novel operational matrix of shifted GPs in the framework of Riemann-Liouville fractional-order integral operator.

Theorem 4.2. *The fractional integral operational matrix corresponding to the Riemann-Liouville definition for order $\alpha \in \mathbb{R}_+$ of shifted GPs as defined in Eq. (3.5), can be obtained by using the following result*

$$_{RL}I^{\alpha}\Lambda(x) \approx E^{(\alpha)}_{(M-1\times M-1)}\Lambda(x),$$

where, $E^{(\alpha)}_{(M-1\times M-1)}$ represents the integral operational matrix defined below

$$\begin{aligned} E^{(\alpha)}_{(M-1\times M-1)} &= \sum_{s=0}^{M-1}\theta_{(s,j)}, \\ \theta_{(s,j)} &= \sum_{k=0}^{s}\sum_{i=0}^{j}\frac{(-1)^{s-k}(-1)^{j-i}\Gamma(s+k+2\mu)(2j+2\mu)(j!)\Gamma(j+i+2\mu)}{(s-k!)(j-i)!i!\Gamma(k+\mu+\frac{1}{2})\Gamma(\alpha+1+k)\Gamma(j+2\mu)} \\ &\quad\times\frac{\Gamma(i+\alpha+k+\mu+\frac{1}{2})}{\Gamma(i+\mu+\frac{1}{2})\Gamma(i+\alpha+k+2\mu+1)}, \quad s,j=0,1,\cdots,M-1. \end{aligned}$$

Proof. For the proof, see [10]. □

Theorem 4.3. *In the Caputo framework, the fractional-order derivative operational matrix of order $\alpha \in \mathbb{R}_+$ of shifted GPs as defined in Eq. (3.5), can be obtained by applying the following result*

$$_{C}\mathcal{D}^{\alpha}\Lambda(x) \approx Q^{(\alpha)}_{(M-1,M-1)}\Lambda(x),$$

where $Q^{(\alpha)}_{(M-1,M-1)}$ represents the derivative operational matrix defined as

$$\begin{aligned} Q^{(\alpha)}_{(M-1,M-1)} &= \sum_{k=\lceil\alpha\rceil}^{e}\vartheta_{(e,f)}, \\ \vartheta_{(e,f)} &= \sum_{k=0}^{e}\sum_{s=0}^{f}\frac{(-1)^{e-k}(-1)^{f-s}\Gamma(e+k+2\mu)(2f+2\mu)(f!)\Gamma(\mu+\frac{1}{2})\Gamma(f+s+2\mu)}{(e-k)!(f-s)!\Gamma(s+\mu+\frac{1}{2})\Gamma(f+2\mu)\Gamma(k+\mu+\frac{1}{2})\Gamma(k-\alpha+1)} \\ &\quad\times\frac{\Gamma(s-\alpha+k+\mu+\frac{1}{2})}{\Gamma(s+k-\alpha+2\mu+1)}. \end{aligned}$$

Proof. For proof, see [15]. □

Theorem 4.4. *Let $\nu(x) \in L^2[0,1]$, it can then be formulated as a series expansion using shifted GPs, i.e., $\nu(x) \approx \sum_{e=0}^{M-1} d_e G^{\mu}_e(x) = \Theta\Lambda(x)$. Let $f : [0,1] \to \mathbb{R}$ be defined by $f(x) = bx^m$, where $b \in \mathbb{R}$, $m \in \mathbb{N}$. Then, the following holds true:*

$$f(x)_0I^{\alpha}_{\eta}\nu(x) = \Theta^{T}_{M-1}\Delta^{(\alpha,m,b)}_{(M-1,M-1)}\Lambda_{M-1}(x), \quad 0<\eta<1,$$

where $\Delta^{(\alpha,m,b)}_{(M-1,M-1)}$ is the operational matrix defined as

$$\Delta^{(\alpha,m,b)}_{(M-1,M-1)} = \sum_{p=0}^{e}A_{(e,p)}\frac{\Gamma(1+p)\eta^{p+\alpha}}{\Gamma(1+p+\alpha)}\sum_{l=0}^{k}\frac{b(-1)^{k-l}\Gamma(k+l+2\mu)\Gamma(2\mu)^2(2k+2\mu)k!}{\Gamma(l+\mu+\frac{1}{2})(k-l)!l!(l+m+1)\Gamma(\mu+\frac{1}{2})^2\Gamma(k+2\mu)}, \tag{4.1}$$

where

$$A_{(e,p)} = \frac{\Gamma(\mu+\frac{1}{2})}{\Gamma(2\mu)}\sum_{p=0}^{e}\frac{(-1)^{e-p}\Gamma(e+p+2\mu)}{\Gamma(p+\mu+\frac{1}{2})(e-p)!e!}.$$

Proof. Since

$$\nu(x) = \sum_{e=0}^{M-1} d_e G_e^{\mu}(x), \tag{4.2}$$

when the Riemann-Liouville fractional integral operator is applied to Eq. (4.2), we obtain the following relation:

$${}_0I_{\eta}^{\alpha}\nu(x) = \sum_{e=0}^{M-1} d_e \left[\sum_{p=0}^{e} A_{(e,p)} \frac{\Gamma(1+p)}{\Gamma(1+p+\alpha)} \eta^{p+\alpha} \right], \tag{4.3}$$

where

$$A_{(e,p)} = \frac{\Gamma(\mu+\frac{1}{2})}{\Gamma(2\mu)} \sum_{p=0}^{e} \frac{(-1)^{e-p}\Gamma(e+p+2\mu)}{\Gamma(p+\mu+\frac{1}{2})(e-p)!e!}.$$

Equation (4.3) can also be expressed as

$$f(x){}_0I_{\eta}^{\alpha}\nu(x) = \sum_{e=0}^{M-1} d_e H_{(e,p)} b x^m. \tag{4.4}$$

$H_{(e,p)}$ is given below

$$H_{(e,p)} = \sum_{p=0}^{e} A_{(e,p)} \frac{\Gamma(1+p)\eta^{p+\alpha}}{\Gamma(1+p+\alpha)}.$$

The expression, $H_{(e,p)} b x^m$ can further be computed using Gegenbauer series as

$$H_{(e,p)} b x^m = \sum_{k=0}^{M-1} D_k G_k^{\mu}(x), \tag{4.5}$$

where

$$\begin{aligned} D_k &= \frac{\Gamma(2\mu)^2(2k+2\mu)k!H_{(e,p)}}{\Gamma(\mu+\frac{1}{2})^2\Gamma(k+2\mu)} \sum_{l=0}^{k} \frac{(-1)^{k-l}\Gamma(k+l+2\mu)b}{\Gamma(l+\mu+\frac{1}{2})(k-l)!l!(l+m+1)} \\ &= \sum_{p=0}^{e} A_{(e,p)} \frac{\Gamma(1+p)\eta^{p+\alpha}}{\Gamma(1+p+\alpha)} \sum_{l=0}^{k} \frac{b(-1)^{k-l}\Gamma(k+l+2\mu)\Gamma(2\mu)^2(2k+2\mu)k!}{\Gamma(l+\mu+\frac{1}{2})(k-l)!l!(l+m+1)\Gamma(\mu+\frac{1}{2})^2\Gamma(k+2\mu)}. \end{aligned}$$

Now inserting Eq. (4.5) in Eq. (4.4), we have

$$\begin{aligned} f(x){}_0I_{\eta}^{\alpha}\nu(x) &= \sum_{e=0}^{M-1}\sum_{k=0}^{M-1} d_e \sum_{p=0}^{e} A_{(e,p)} \frac{\Gamma(1+p)\eta^{p+\alpha}}{\Gamma(1+p+\alpha)} \\ &\quad \times \sum_{l=0}^{k} \frac{b(-1)^{k-l}\Gamma(k+l+2\mu)\Gamma(2\mu)^2(2k+2\mu)k!}{\Gamma(l+\mu+\frac{1}{2})(k-l)!l!(l+m+1)\Gamma(\mu+\frac{1}{2})^2\Gamma(k+2\mu)} G_k^{\mu}(x) \\ &= \sum_{e=0}^{M-1}\sum_{k=0}^{M-1} d_e \Delta_{(M-1,M-1)}^{(\alpha,m,b)} G_k^{\mu}(x). \end{aligned} \tag{4.6}$$

The expression (4.6) in matrix form can be written as

$$f(x)\,{}_0I_\eta^\alpha \nu(x) = \Theta_{M-1}^T \Delta_{(M-1,M-1)}^{(\alpha,m,b)} \Lambda_{M-1}(x).$$

As given in Eq. (4.1), $\Delta_{(M-1,M-1)}^{(\alpha,m,b)}$ satisfies the required expression, thereby proving the result, where,

$$\Delta_{(5,5)}^{(1,1,1)} = \begin{pmatrix} 0.5000 & 0.2500 & 0 & 0 & 0 \\ 0 & 0 & 0 & 0 & 0 \\ 0.1667 & 0.0833 & 0 & 0 & 0 \\ 0 & 0 & 0 & 0 & 0 \\ 0.1000 & 0.0500 & 0 & 0 & 0 \end{pmatrix}, \qquad \Delta_{(5,5)}^{(1.5,1,1)} = \begin{pmatrix} 0.3761 & 0.1881 & 0 & 0 & 0 \\ -0.1505 & -0.0752 & 0 & 0 & 0 \\ 0.0967 & 0.0484 & 0 & 0 & 0 \\ -0.0716 & -0.0358 & 0 & 0 & 0 \\ 0.0570 & 0.0285 & 0 & 0 & 0 \end{pmatrix},$$

$$\Delta_{(5,5)}^{(1.9,1,1)} = \begin{pmatrix} 0.2736 & 0.1368 & 0 & 0 & 0 \\ -0.1698 & -0.0849 & 0 & 0 & 0 \\ 0.0854 & 0.0427 & 0 & 0 & 0 \\ -0.0695 & -0.0347 & 0 & 0 & 0 \\ 0.0516 & 0.0258 & 0 & 0 & 0 \end{pmatrix}, \qquad \Delta_{(5,5)}^{(2,1,1)} = \begin{pmatrix} 0.2500 & 0.1250 & 0 & 0 & 0 \\ -0.1667 & -0.0833 & 0 & 0 & 0 \\ 0.0833 & 0.0417 & 0 & 0 & 0 \\ -0.0667 & -0.0333 & 0 & 0 & 0 \\ 0.0500 & 0.0250 & 0 & 0 & 0 \end{pmatrix}.$$

□

Remark 4.5. Consider $f(x) = bx^m$ together with approximation $\nu(x) \approx \sum_{e=0}^{M-1} d_e G_e^\mu(x) = \Theta_{M-1}^T \Lambda_{M-1}(x)$; then the following relation holds

$$f(x)\Theta_{M-1}^T E_{(M-1,M-1)}^{(\alpha)} \Lambda_{M-1}(\eta) \approx \Theta_{M-1}^T \Delta_{(M-1,M-1)}^{(\alpha,m,b)} \Lambda_{M-1}(x).$$

5. Numerical method

This part of the study introduces a numerical scheme for handling FODEs under TPBCs. The method employs derivative and integral matrices derived from shifted GPs. Through this construction, the original FODEs are reformulated into matrix equations of the Sylvester form, which can be addressed effectively with the aid of numerical computation tools. Consider the FODEs with TPBCs:

$${}_C\mathcal{D}^{\alpha_0} Y(x) = a_1\,{}_C\mathcal{D}^{\beta_0} Y(x) + a_2 Y(x) + F(x), \quad x \in [0,1], \quad Y(0) = p_0, \quad Y(1) = p_1, \tag{5.1}$$

where the Caputo fractional-order derivative is representing by ${}_C\mathcal{D}$ with $0 < \beta 0 < \alpha_0 \leqslant 2$. Here, real constants are a_1, a_2, p_0, and p_1 and $F(x)$ is representing a source term. The function $Y(x)$ denotes the solution to problem (1.1). Let us suppose that

$$\mathcal{D}^{\alpha_0} Y(x) = \Theta_{M-1}^T \Lambda_{M-1}(x). \tag{5.2}$$

By applying the Riemann-Liouville fractional integral to Eq. (5.2) and utilizing Theorems 4.2 and 4.4, together with the TPBCs in Eq. (5.1), the following result is obtained:

$$Y(x) = \Theta_{M-1}^T E_{(M-1,M-1)}^{(\alpha_0)} \Lambda_{M-1}(x) - \Theta_{M-1}^T \Delta_{(M-1,M-1)}^{(\alpha_0,m,b)} \Lambda_{M-1}(x) + R_{M-1}^T \Lambda_{M-1}(x), \tag{5.3}$$

where $R_M^T = p_0 + (p_1 - p_0)x$. Equation (5.3) can also be written as

$$Y(x) = \Theta_{M-1}^T \left(E_{(M-1,M-1)}^{(\alpha_0)} - \Delta_{(M-1,M-1)}^{(\alpha_0,m,b)} \right) \Lambda_{M-1}(x) + R_{M-1}^T \Lambda_{M-1}(x). \tag{5.4}$$

Using Eq. (5.4) and Theorem 4.3, the derivative term, ${}_C\mathcal{D}^{\beta_0} Y(x)$ in Eq. (5.1) can be approximated as

$$\begin{aligned} {}_C\mathcal{D}^{\beta_0} Y(x) = \Theta_{M-1}^T &\left(E_{(M-1,M-1)}^{(\alpha_0)} - \Delta_{(M-1,M-1)}^{(\alpha_0,m,b)} \right) Q_{(M-1,M-1)}^{(\beta_0)} \Lambda_{M-1}(x) \\ &+ R_{M-1}^T Q_{(M-1,M-1)}^{(\beta_0)} \Lambda_{M-1}(x). \end{aligned} \tag{5.5}$$

By substituting Eq. (5.2), Eq. (5.4), and Eq. (5.5) in Eq. (5.1), we have

$$\begin{aligned}&\Theta_{M-1}^{T}\Lambda_{M-1}(x)\\&= a_1\,\Theta_{M-1}^{T}\Big(E_{(M-1,M-1)}^{(\alpha_0)}-\Delta_{(M-1,M-1)}^{(\alpha_0,m,b)}\Big)Q_{(M-1,M-1)}^{(\beta_0)}\Lambda_{M-1}(x)+a_1\,R_{M-1}^{T}Q_{(M-1,M-1)}^{(\beta_0)}\Lambda_{M-1}(x)\\&\quad+a_2\,\Theta_{M-1}^{T}\Big(E_{(M-1,M-1)}^{(\alpha_0)}-\Delta_{(M-1,M-1)}^{(\alpha_0,m,b)}\Big)\Lambda_{M-1}(x)+a_2\,R_{M-1}^{T}\Lambda_{M-1}(x)+\Phi_{M-1}^{T}\Lambda_{M-1}(x),\end{aligned}\tag{5.6}$$

where $F(x)=\Phi_{M-1}^{T}\Lambda_{M-1}(x)$. Equation (5.6) can also be expressed as

$$\begin{aligned}&\Theta_{M-1}^{T}-\Theta_{M-1}^{T}\left(a_1\left(E_{(M-1,M-1)}^{(\alpha_0)}-\Delta_{(M-1,M-1)}^{(\alpha_0,m,b)}\right)Q_{(M-1,M-1)}^{(\beta_0)}+a_2\left(E_{(M-1,M-1)}^{(\alpha_0)}-\Delta_{(M-1,M-1)}^{(\alpha_0,m,b)}\right)\right)\\&=a_1R_{M-1}^{T}Q_{(M-1,M-1)}^{(\beta_0)}+a_2R_{M-1}^{T}+\Phi_{M-1}^{T}.\end{aligned}\tag{5.7}$$

Since Eq. (5.7) is a Sylvester-type equation, it can be directly solved for the unknown Θ_{M-1}^{T}, and the solution to problem 5.1 is then obtained by substituting these values into Eq. (5.4).

6. Error estimation

Consider the weight function $w(x)=(x-x^2)^{\mu-\frac{1}{2}}$ defined on the interval $[0,1]$. This function represents a non-negative integrable function over the given domain. Let $L_w^2\in[0,1]$ denote the weighted space consisting of functions $Y:[0,1]\to\mathbb{R}$, such that

$$L_w^2=L_w^2[0,1]=\{Y:[0,1]\to\mathbb{R}\text{ such that }\int_0^1|Y(x)|^2w(x)dx<\infty\}.$$

Let Λ_{M-1} be a closed, finite-dimensional subspace of $L_w^2[0,1]$, constructed from the basis consisting of the first $M-1$ shifted GPs, i.e., $\Lambda_{M-1}=\{G_0^{\mu},G_1^{\mu},\dots,G_{M-1}^{\mu}\}$. For any function $Y(x)\in L_w^2[0,1]$, there exists a unique best approximation $\hat{Y}_{M-1}(x)\in\Lambda_{M-1}$, which implies

$$\|Y(x)-\hat{Y}_{M-1}(x)\|w\leqslant\|Y-\psi\|w,\text{ for all }\psi\in\Lambda_{M-1}.$$

Furthermore, if $\hat{Y}_{M-1}(x)\in\Lambda_{M-1}$, it can be expressed as

$$\hat{Y}_{M-1}(x)=\sum_{q=0}^{M-1}a_qG_q^{\mu}=\Theta_{M-1}^{T}\Lambda_{M-1}(x).$$

The coefficients a_q in the series are determined from Eq. (3.4).

Lemma 6.1. *Let* $\Lambda_{M-1}=\left[G_0^{\mu},G_1^{\mu},\dots,G_{M-1}^{\mu}\right]$ *and consider* $Y(x)\in C^{M-1}[0,1]$, *where* $Y:[0,1]\to\mathbb{R}$. *If* $\hat{Y}_{M-1}(x)$ *denotes the best approximation from the subspace* Λ_{M-1}, *it can be expressed as* $\hat{Y}_{M-1}(x)=\sum_{q=0}^{M-1}a_qG_q^{\mu}=\Theta_{M-1}^{T}\Lambda_{M-1}(x)$. *The norm gives the error bound for this approximation*

$$\|Y(x)-\hat{Y}_{M-1}(x)\|_w\leqslant\frac{\kappa^2H^{2(M-1)}\Gamma^2(\mu+\frac{1}{2})}{((M-1)!)^2\Gamma(2\mu+1)},$$

where $\kappa=\max_{x\in[0,1]}\left(\hat{Y}^{(M-1)}(x)\right)$ *and* $H=\max\{1-x,x\}$.

Proof. Assume $Y(x)$ is a real-valued function that is continuously $M-1$ times differentiable. The function $Y(x)$ admits a power series expansion centered at $x=p$, which can be written as:

$$z(x)=\sum_{q=0}^{M-1}\frac{(x-p)^q}{q!}Y^{(q)}(n).$$

This series converges within the radius of convergence, which is determined by the properties of $Y(x)$ and its derivatives at the point $x = p$ with the following error bound

$$|Y(x) - z(x)| = \left| \hat{Y}^{(M-1)}(\gamma) \frac{(x-p)^{M-1}}{(M-1)!} \right|, \ p < \gamma < 1, \ \leqslant \kappa \frac{(x-p)^{M-1}}{(M-1)!}.$$

Since $\hat{Y}_{M-1}(x)$ is the best approximation from Λ_{M-1} and $z(x) \in \Lambda_{M-1}$, we have

$$\begin{aligned} \|Y(x) - \hat{Y}_{M-1}(x)\|_w^2 &\leqslant \|Y(x) - z(x)\|_w^2 \\ &= \int_0^1 (Y(x) - z(x))_w^2 w(x) dx \leqslant \frac{\kappa^2}{((M-1)!)^2} \int_0^1 (x-p)^{2(M-1)} w(x) dx. \end{aligned} \tag{6.1}$$

Since $H = \max\{1-x, x\}$; the maximum distance of x from the end points of the interval $[0,1]$. Therefore, $|x-p| \leqslant H$, for all $x \in [0,1]$. Consequently, we have

$$(x-p)^{2(M-1)} \leqslant H^{2(M-1)}. \tag{6.2}$$

By using Eq. (6.2) into Eq. (6.1), we have

$$\|Y(x) - \hat{Y}_{M-1}(x)\|_w^2 \leqslant \frac{\kappa^2 H^{2(M-1)}}{((M-1)!)^2} \int_0^1 (x-x^2)^{\mu-\frac{1}{2}} dx, \tag{6.3}$$

where $w(x) = (x-x^2)^{\mu-\frac{1}{2}}$ denotes a non-negative function, integrable over $[0,1]$. By using substitution, $x = \sin^2(\theta)$ and by using the following definition of the Beta function along with the result, $B(a,b) = \frac{\Gamma(a)\Gamma(b)}{\Gamma(a+b)}$,

$$B(a,b) = \int_0^1 x^{a-1}(1-x)^{b-1} dx,$$

Eq. (6.3) can be simplified as

$$\|Y(x) - \hat{Y}_{M-1}(x)\|_w^2 \leqslant \frac{\kappa^2 H^{2(M-1)} \Gamma^2(\mu + \frac{1}{2})}{((M-1)!)^2 \Gamma(2\mu+1)}.$$

Hence the result is proven. □

7. Examples

This section presents a detailed evaluation of the PM through the solution of various illustrative examples. The results are then compared with those reported in the literature, with the comparative findings displayed through tables and graphical plots.

Example 7.1. Consider the following fractional order problem with TPBCs [3],

$${}_C\mathcal{D}^{\alpha_0} Y(x) + {}_C\mathcal{D}^{\beta_0} Y(x) + Y(x) = F(x), \ \ 1 < \beta_0 < \alpha_0 \leqslant 2, \ \ x \in [0,5], \quad Y(0) = p_0, \ Y(5) = p_1.$$

The exact solution of Example 7.1 at $\alpha_0 = 2$, $\beta_0 = \frac{3}{2}$,$p_0 = 0$, $p_1 = 25$, and $F(x) = x^2 + 2 + 4\sqrt{\frac{x}{\pi}}$ exists. The exact solution is given as $Y(x) = x^2$. Figure 2 depicts the exact and approximate solutions of Example 7.1 computed at various values of M, illustrating the convergence of the approximate solution towards the exact solution. Figure 3 illustrates the absolute error for $M = 4$, indicating that the approximate solution matches the exact solution with an accuracy of up to 19 decimal places. The absolute error between the exact and approximate solutions lies within the range of 10^{-14} to 10^{-19}, reflecting the high precision of the approximate results obtained using PM. Figure 4 illustrates the L_2 error norm, demonstrating excellent accuracy and consistency across various μ values for $M = 4$. This provides information about the error reduction rate as the algorithm progresses, thereby validating its effectiveness in approximating the exact solution.

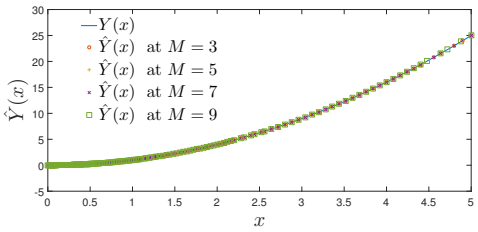

Figure 2: Approximate and Exact solution plots for Example 7.1 corresponding to different M values.

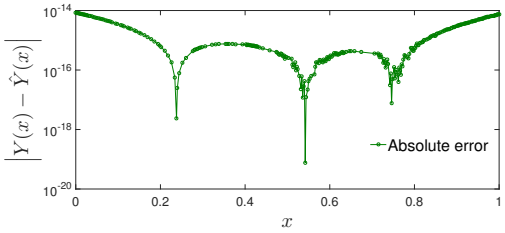

Figure 3: The Absolute error plot of Example 7.1 computed using PM at $M = 4$.

Example 7.2. Consider the following fractional order problem with TPBCs [36]

$$ {}_C\mathcal{D}^{\alpha_0}Y(x) + {}_C\mathcal{D}^{\beta_0}Y(x) + Y(x) = F(x), \quad 1 < \beta_0 < \alpha_0 \leqslant 2, \; x \in [0,1], \quad Y(0) = p_0, \; Y(1) = p_1. $$

The exact solution of Example 7.2 at $\alpha_0 = 2$, $\beta_0 = \frac{3}{2}$, $p_0 = 1$, $p_1 = 2$, and $F(x) = 1 + x$ is given as $Y(x) = 1 + x$. The approximate and exact solutions of Example 7.2 are depicted in Figure 5 for various values of M, demonstrating that the approximate solution aligns with the exact solution. The L_2 error norm is presented in Figure 6 for $M = 9$ and $M = 10$ with different values of μ, highlighting excellent accuracy and consistency across various μ values for $M = 9$ and $M = 10$. This provides information about the error reduction rate as the algorithm progresses, thereby validating its effectiveness in approximating the exact solution. Table 1 presents a comparison of the absolute error between our PM and the BCM [36]. Our PM shows significantly enhanced compatibility results compared to the BCM [36], particularly at smaller scales. Additionally, the PM yields excellent results across the entire domain, in contrast to the BCM, where the absolute error increases significantly at $x = 0.9$ (see Table 1). This demonstrates that the PM is globally convergent.

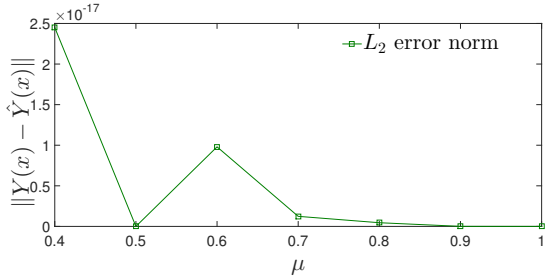

Figure 4: L_2 error norm plot of Example 7.1 calculated via the PM at $M = 4$ across different μ values.

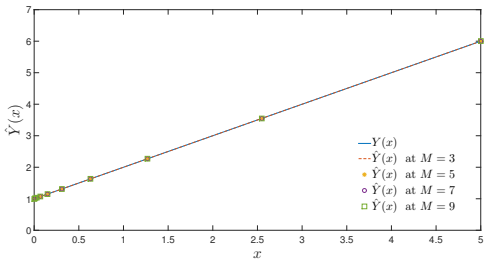

Figure 5: Exact and approximate solutions plots for Example 7.2 at different values of M.

Table 1: Comparison of absolute errors for Example 7.2.

x	PM at $M = 3$, $\mu = 0.5$	PM at $M = 4$, $\mu = 0.5$	BCM at $M = 6$, $\alpha = 0.5$, [36]
0.0	0	0	0
0.1	0	1.812×10^{-16}	6.1919×10^{-16}
0.2	0	1.150×10^{-15}	1.0292×10^{-15}
0.3	0	1.246×10^{-15}	1.4779×10^{-15}
0.4	0	1.775×10^{-15}	1.9697×10^{-15}
0.5	0	2.412×10^{-15}	2.4941×10^{-15}
0.6	0	2.833×10^{-15}	3.0365×10^{-15}
0.7	0	2.714×10^{-15}	3.5805×10^{-15}
0.8	0	1.731×10^{-15}	4.1090×10^{-15}
0.9	0	4.420×10^{-16}	4.6047×10^{-8}
1.0	0	4.128×10^{-15}	5.0500×10^{-15}

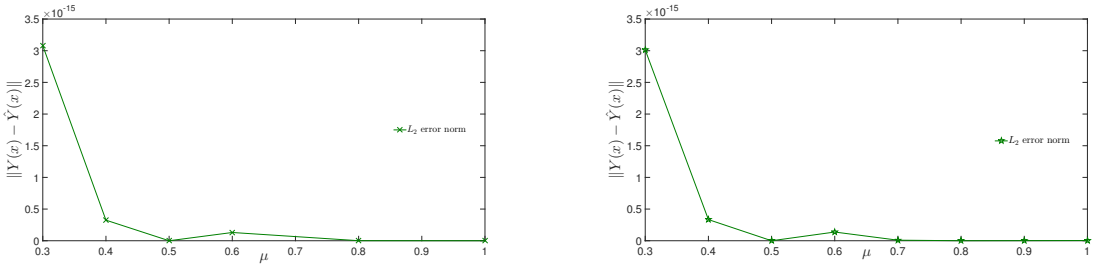

a. $M = 9$ b. $M = 10$

Figure 6: L_2 error norm plots for Example 7.2, calculated via PM at various μ and M values.

Example 7.3. Consider the following fractional order problem with TPBCs [32, 33, 36]

$$ {}_C\mathcal{D}^{\alpha_0} Y(x) + \frac{8}{17} {}_C\mathcal{D}^{\beta_0} Y(x) + \frac{13}{51} Y(x) = F(x), \quad 1 < \beta_0 < \alpha_0 \leqslant 2, \quad x \in [0,1], \quad Y(0) = 0, \quad Y(1) = 0. $$

The exact solution of Example 7.3 at $\alpha_0 = 2$, $\beta_0 = \frac{3}{2}$, and $F(x) = \frac{x^{\frac{-1}{2}}}{89250\sqrt{\pi}} \left[48g(x) + 7\sqrt{x}h(x)\right]$ is provided as

$$ Y(x) = x^5 - \frac{29x^4}{10} + \frac{76x^3}{25} - \frac{339x^2}{250} + \frac{27x}{125}, $$

where $g(x) = 16000x^4 - 32480x^3 + 21280x^2 - 4746x + 189$ and $h(x) = 3250x^5 - 9425x^4 + 264880x^3 + 448107x^2 + 233262x - 34578$. Table 2 shows the comparison of absolute errors between our PM, BCM [36], and HWM [33]. Our analysis indicates that our PM performs significantly better than both the BCM and HWM in terms of accuracy and efficiency, as shown by our results. Figure 7 illustrates the absolute error comparison of our PM with HWM [33] and BCM [36], highlighting that the PM consistently achieves the lowest errors across the entire range of time t. Figure 8 displays the L_2 error norm across different values of M, highlighting excellent accuracy and consistency across various M. This provides information about the error reduction rate as the algorithm progresses, thereby validating its effectiveness in approximating the exact solution. In addition, the PM consistently achieves errors of the order 10^{-13} across the entire domain, indicating high accuracy and strong numerical stability. In contrast, the BCM shows relatively larger errors, particularly at $x = 0.1$ and $x = 0.2$, where the errors are of order 10^{-2} and 10^{-3}, respectively. Although the BCM achieves smaller errors at specific points (e.g., $x = 0.4, 0.6, 0.9$), its performance is inconsistent compared to the uniform accuracy of the PM. Similarly, the HWM performs better than the BCM in some regions, yet its errors remain several orders of magnitude larger than those of the PM, ranging between 10^{-3} and 10^{-4}. Overall, the PM not only provides the smallest absolute errors but also maintains global convergence throughout the domain.

Table 2: Comparison of absolute error for Example 7.3 at $M = 8$.

x	PM	BCM [36]	HWM [33]
0.1	7.62×10^{-13}	1.0800×10^{-2}	3.59748×10^{-4}
0.2	1.04×10^{-13}	8.9595×10^{-3}	1.5829×10^{-3}
0.3	8.81×10^{-13}	3.7797×10^{-3}	1.7866×10^{-3}
0.4	1.23×10^{-13}	1.4413×10^{-7}	1.63436×10^{-3}
0.5	1.41×10^{-13}	1.0001×10^{-3}	1.15787×10^{-3}
0.6	9.46×10^{-13}	6.6150×10^{-8}	5.83561×10^{-4}
0.7	5.64×10^{-13}	1.2599×10^{-3}	1.27102×10^{-4}
0.8	7.63×10^{-13}	1.2800×10^{-3}	1.19676×10^{-4}
0.9	3.17×10^{-13}	2.0656×10^{-8}	5.54006×10^{-4}

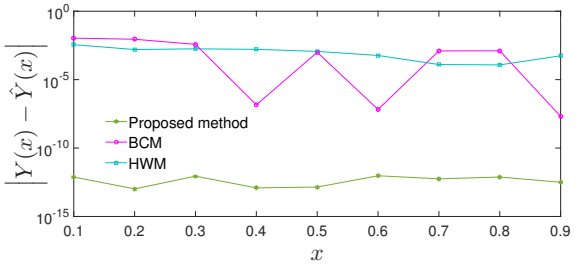

Figure 7: Absolute errors comparison for Example 7.3 calculated using the PM and those from BCM [36] and HWM [33] for $M = 8$.

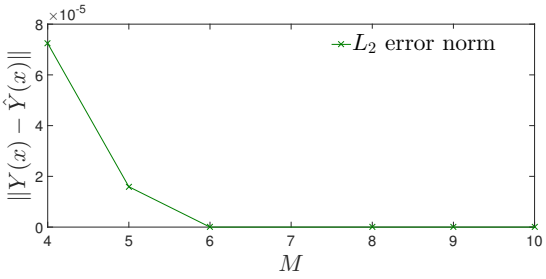

Figure 8: L_2 error norm plots for Example 7.3 calculated via PM at different M values.

Example 7.4. Consider the fractionally damped mechanical oscillator equation subject to TPBCs [25, 33]

$$ {}_C\mathcal{D}^{\alpha_0}Y(x) + {}_C\mathcal{D}^{\beta_0}Y(x) + \frac{-1}{\sqrt{(\pi)}}Y(x) = F(x), \quad 0 < \beta_0 < \alpha_0 < 2, \; x \in [0,1], \quad Y(0) = p_0, \quad Y(1) = p_1. \tag{7.1} $$

The exact solution of Example 7.4 at $\alpha_0 = 7/4$, $\beta_0 = 1/2$, $p_0 = 0 = p_1$, and $F(x) = \frac{1}{\sqrt{\pi}}\left[\frac{16x^{\frac{3}{2}}g(x)}{45045} + \frac{24x^{\frac{1}{4}}h(x)}{9945\Gamma(\frac{5}{4})} - x^2(5x-3)^2 r(x)\right]$ is provided below

$$ Y(x) = 625x^7 - 2000x^6 + 2450x^5 - 1420x^4 + 381x^3 - 36x, $$

where $g(x) = 28028000x^3 - 14620320x^2 - 21527571x - 270270$, $h(x) = \frac{1}{4}6400000x^5 - 15360000x^4 + 13328000x^3 - 5021120x^2 + 757809x - 29835$, and $r(x) = 25x^3 - 50x^2 + 29x - 4$. When $\alpha_0 = 2$ and $\beta_0 = 1$, Eq. (7.1) reduces to the classical differential equation governing a harmonic oscillator. Palfalvi [25] employed the Adomian decomposition technique to study a mechanically damped oscillator under fractional damping and sinusoidal excitation.

A detailed comparison of the absolute errors is given in Table 3 for Example 7.4 using PM and the HWM [33] at $M = 8$ and $M = 16$. The table displays absolute errors at various values of x, highlighting the performance difference between the two methods. Across all domain points at $M = 8$ and $M = 16$, our PM consistently exhibits lower absolute errors compared to HWM. Figure 9 shows a comparison of the exact solution with our approximate solution at various values of M. It is evident that by increasing the value of M, the approximate solution using PM progressively converges towards the exact solution of Example 7.4. The L_2 error norm is shown in Figure 10 demonstrating the accuracy of our algorithm at various values of M. It is evident that the value of M increases, the error decreases significantly, and eventually approaches zero. Consequently, this behavior confirms the efficiency of our PM in solving problems with TPBCs.

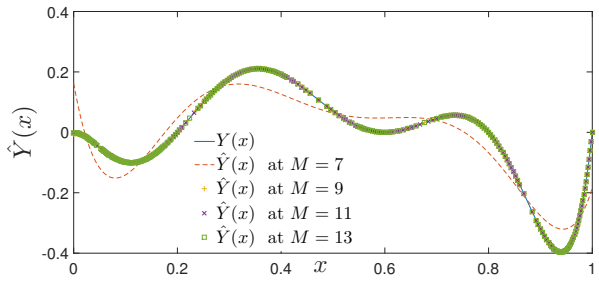

Figure 9: Plots of the exact and approximate solutions for Example 7.4 with different values of M.

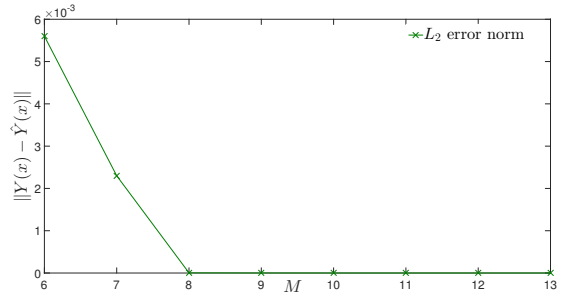

Figure 10: L_2 error norm plots for Example 7.4 computed PM at different M values.

Table 3: Comparison of absolute error corresponding to Example 7.4 for $M = 8$ and $M = 16$.

x	PM at $M = 8$	HWM[33] at $M = 8$	PM at $M = 16$	HWM[33] at $M = 16$
0.1	9.2×10^{-3}	4.0484×10^{-2}	6.242×10^{-6}	1.01858×10^{-3}
0.2	3.1×10^{-3}	1.7310×10^{-2}	1.667×10^{-6}	1.81594×10^{-4}
0.3	2.01×10^{-3}	1.0302×10^{-2}	6.410×10^{-7}	1.45503×10^{-3}
0.4	4.0×10^{-3}	3.190×10^{-3}	9.780×10^{-7}	5.00849×10^{-4}
0.5	2.6×10^{-3}	2.6157×10^{-2}	2.800×10^{-8}	7.38950×10^{-4}
0.6	1.7×10^{-3}	3.9802×10^{-2}	9.090×10^{-7}	5.94033×10^{-5}
0.7	1.1×10^{-3}	2.0226×10^{-2}	1.740×10^{-7}	1.01475×10^{-4}
0.8	1.1×10^{-3}	1.8284×10^{-2}	7.350×10^{-7}	3.44832×10^{-3}
0.9	1.14×10^{-3}	2.95680×10^{-2}	6.400×10^{-8}	4.65424×10^{-3}

Example 7.5. Consider the following FODEs having non-polynomial solutions with TPBCs [33, 35]

$$ {}_C\mathcal{D}^{\alpha_0} Y(x) + a_1 {}_C\mathcal{D}^{\beta_0} Y(x) + a_2 Y(x) = F(x),\ 1 \leqslant \beta_0 < \alpha_0 \leqslant 2,\ x \in [0,1],\ \ Y(0) = p_0,\ \ Y(1) = p_1. $$

Example 7.5 has the exact solution at $\alpha_0 = 2$, $\beta_0 = 1$, $p_0 = 0$, $p_1 = 0$, $a_1 = -1$, $a_2 = 0$, and $F(x) = -e^{x-1} - 1$ is given as $Y(x) = x(1 - e^{x-1})$. Table 4 presents a comparison of the approximate solutions obtained using the PM, HWM [33], and fourth-order HPGF [35] against the exact solution for Example 7.5. The PM demonstrates excellent accuracy, with its results matching the exact solution up to machine precision across the entire domain. The HWM also performs well and remains close to the exact solution, but it exhibits slightly larger deviations than the PM, particularly at intermediate values of x. In contrast, the HPGF shows noticeable discrepancies, especially near $x = 0.4$ to $x = 0.8$, where its approximations deviate more significantly from the exact solution. Figure 11 further illustrates the superior convergence of the PM, as increasing M enhances the accuracy of the approximation until it coincides with the exact solution. Moreover, the L_2 error norm in Figure 12 confirms that the error associated with the PM diminishes rapidly with increasing M, approaching zero. These observations highlight the robustness and global convergence of the PM, while revealing the relative weaknesses of HWM and HPGF in maintaining accuracy throughout the domain.

Table 4: Approximate solution comparison of Example 7.5 using PM, HWM [33], and HPGF [35].

x	PM at $M = 8$	HWM [33]	Fourth order HPGF [35]	Exact solution
0	0.00000000	——	——	0.00000000
0.1	0.05934303	0.05934300	0.05934820	0.05934303
0.2	0.11013421	0.11013418	0.11014318	0.11013421
0.3	0.15102441	0.15102438	0.15103441	0.15102441
0.4	0.18046535	0.18047531	0.18048329	0.18046535
0.5	0.19673467	0.19673463	0.19673826	0.19673467
0.6	0.19780797	0.19780792	0.19780653	0.19780797
0.7	0.18142725	0.18142718	0.18142196	0.18142725
0.8	0.14501540	0.14501532	0.14500893	0.14501540
0.9	0.08564632	0.08564623	0.08564186	0.08564632
1.0	0.00000000	——	——	0.00000000

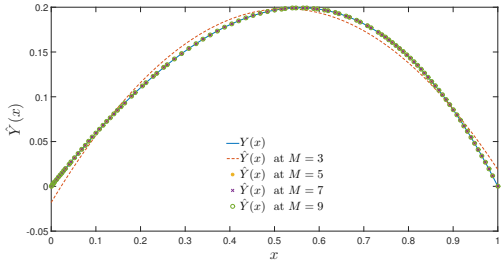

Figure 11: Plots of the exact and approximate solutions for Example 7.5 with different values of M.

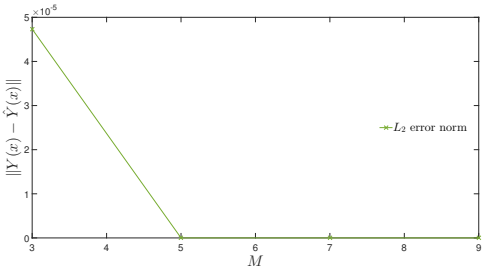

Figure 12: L_2 error norm plot corresponding to Example 7.5, calculated via PM at different M values.

Example 7.6. Consider the following FODEs having non-polynomial solution with TPBCs [33, 35]

$$ {}_C\mathcal{D}^{\alpha_0}Y(x) + a_1{}_C\mathcal{D}^{\beta_0}Y(x) + a_2Y(x) = F(x),\ 1 \leqslant \beta_0 < \alpha_0 \leqslant 2,\ x \in [0,1],\quad Y(0) = p_0,\quad Y(1) = p_1. $$

Example 7.6 has the exact solution at $\alpha_0 = 2$, $\beta_0 = 1$ $p_0 = 1$, $p_1 = -1$, $a_1 = 1$, $a_2 = -\pi^2$, and $F(x) = -\pi\sin(\pi x)$ is given as $Y(x) = \cos(\pi x)$. In Figure 13, we present the exact and approximated solutions across various values of M. The plots, evolving with varying M, resemble sinusoidal oscillating waves. Our PM performs exceptionally well with problems involving trigonometric function solutions, as the approximate solution closely aligns with the exact solution of Example 7.6. We also computed the absolute errors across different x and M. At $M = 5$, Figure 14 shows elongated wavelength shapes. However, increasing M to 7 shortens the wavelengths, indicating decreased error. At $M = 11$ and $M = 17$, the wavelengths become more tightly packed, demonstrating the increased detail and accuracy achieved by our PM.

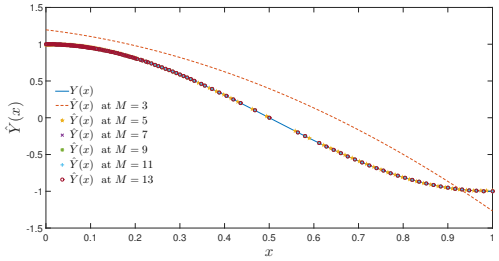

Figure 13: Exact and approximate solution plots for Example 7.6 corresponding to different M values.

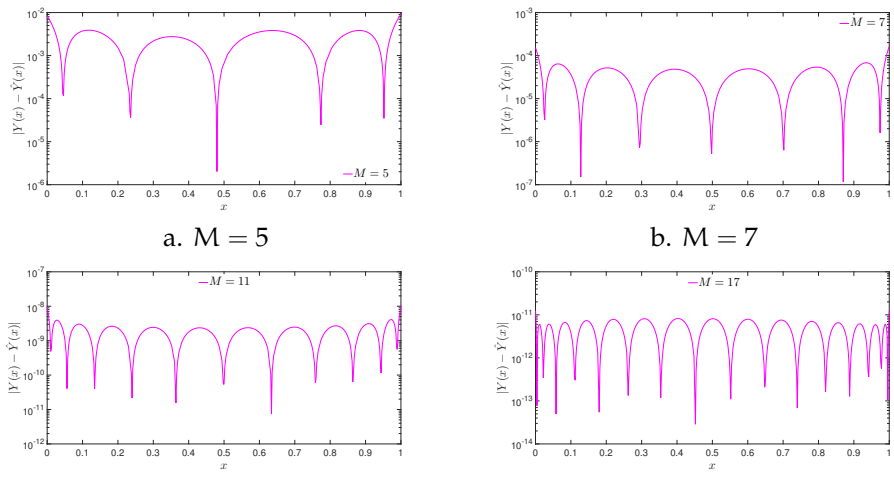

a. $M = 5$ b. $M = 7$

c.$M = 11$ d. $M = 17$

Figure 14: Plot of absolute errors corresponding to Example 7.6 calculated by using the PM at different values of M.

Example 7.7. Consider the following FODEs having non-polynomial solution with TPBCs [4]

$$ {}_C\mathcal{D}^{2\alpha_0}Y(x) + a_1 {}_C\mathcal{D}^{\beta_0}Y(x) + a_2 Y(x) = F(x), \quad 0 < \beta_0 < \alpha_0 \leqslant 1, \quad x \in [0,1], \quad Y(0) = p_0, \quad Y(1) = p_1. $$

Example 7.7 has the exact solution at $\alpha_0 = 1$, $\beta_0 = 1$ $p_0 = 0$, $p_1 = 0$, $a_1 = 5$, $a_2 = 4$, and $F(x) = 1$ is given as

$$ Y(x) = \left(\frac{e^{-3} - e}{4(1 - e^{-3})} \right) e^{-x} + \left(-\frac{1}{4} - \frac{e^{-3} - e}{4(1 - e^{-3})} \right) e^{-4x} + \frac{1}{4}. $$

The method proposed in [4] is built upon FCFCD of order α_0 and $2\alpha_0$, and its stability and efficiency were demonstrated through several examples. However, the error analysis in Table 5 shows that while their approach performs reasonably well for fractional-order cases (e.g., $\alpha_0 = 0.8$), it is less effective for integer-order cases ($\alpha_0 = 1$), where the error stagnates around 10^{-3}. In contrast, our PM achieves errors of order 10^{-7} to 10^{-6} in the same setting, confirming its superior accuracy and convergence. Even for fractional orders, although [4] achieves smaller deviations in the mid-domain, the PM performs better near the endpoints and at $x = 0.9$. This comparison highlights that PM is more efficient and reliable, particularly when transitioning between fractional and integer-order problems, while the method of [4] shows limitations in maintaining accuracy for higher-order cases. Figure 15 shows how the approximate solution achieved using PM progressively converges towards the exact solution of Example 7.7 as M increases, demonstrating the method's effectiveness in solving problems with non-polynomial solutions across different values of M. Furthermore, Figure 16 shows the variation of the L_2 error norm with respect to the parameter M. At $M = 4$, the error norm is approximately 2.4×10^{-5}, and it decreases dramatically as M increases. By $M = 6$, the error essentially drops to zero and remains at this level for all higher values of M up to $M = 12$. This behavior confirms the rapid convergence of the proposed method, as only a relatively small value of M is sufficient to achieve very high precision. The figure demonstrates the efficiency and stability of the PM, since the error does not increase again for larger M but remains negligible.

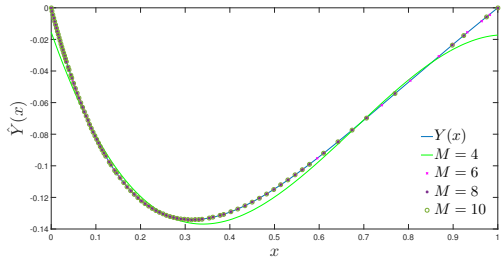

Figure 15: Plots of the exact and approximate solutions for Example 7.7 with different values of M.

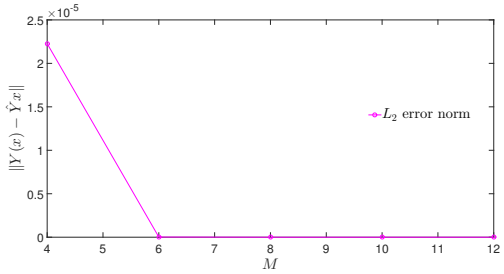

Figure 16: L_2 error norm of Example 7.7 calculated by our PM for different M values

Example 7.8. Consider the following FODEs with TPBCs [9, 12]

$$ {}_C\mathcal{D}^{\alpha_0}Y(x) + a_1 {}_C\mathcal{D}^{\beta_0}Y(x) + a_2 Y(x) = F(x), \quad 1 < \alpha_0 \leqslant 2, \quad x \in [0,1], \quad Y(0) = p_0, \quad Y(1) = p_1. $$

Example 7.8 has the exact solution at $p_0 = 0$, $p_1 = 0$, $a_1 = 0$, $a_2 = 1$, and $F(x) = \frac{2x^{2-\alpha_0}}{\Gamma(3-\alpha_0)}$ is given as $Y(x) = x^2 - x$. Table 6 provides a comparative study of absolute errors for Example 7.8, considering our PM, PSM reported in [12], and GABMM from [9]. For consistency, PM and PSM results are presented at $M = 10$, while GABMM results are reported at $M = 6$ with two different step sizes ($h = \frac{1}{20}$ and $h = \frac{1}{320}$). A key observation is that the PSM results are available only at the boundary point $x = 1$, limiting their applicability for a full comparison across the interval. Similarly, GABMM requires relatively small step sizes to achieve reasonable accuracy, which significantly increases the computational burden. In contrast,

Table 5: Error analysis: PM vs method proposed in [4].

x	PM Error at $\alpha_0 = 0.8$	PM Error at $\alpha_0 = 1$	Error [4] at $\alpha_0 = 0.8$	Error [4] at $\alpha_0 = 1$
0.0	0.0000	0.0000	0.0000	0.0000
0.1	2.63×10^{-2}	9.1×10^{-7}	2.31×10^{-2}	4.00×10^{-3}
0.2	4.97×10^{-2}	1.95×10^{-6}	3.62×10^{-2}	4.00×10^{-3}
0.3	6.13×10^{-2}	1.21×10^{-6}	4.05×10^{-2}	4.00×10^{-3}
0.4	6.27×10^{-2}	5.90×10^{-7}	3.88×10^{-2}	4.00×10^{-3}
0.5	5.77×10^{-2}	2.26×10^{-6}	3.35×10^{-2}	4.20×10^{-3}
0.6	4.87×10^{-2}	1.70×10^{-7}	2.63×10^{-2}	3.80×10^{-3}
0.7	3.71×10^{-2}	7.00×10^{-7}	1.85×10^{-2}	4.00×10^{-3}
0.8	2.45×10^{-2}	2.64×10^{-6}	1.11×10^{-2}	4.00×10^{-3}
0.9	1.22×10^{-3}	1.20×10^{-6}	4.80×10^{-3}	4.00×10^{-3}
1.0	0.0000	0.0000	0.0000	0.0000

our PM not only provides error estimates across the entire interval $[0, 1]$ but also achieves a markedly smaller absolute error at the boundary point $x = 1$ (7.520×10^{-6}), compared to 6.83×10^{-4} for PSM and 3.42×10^{-3} / 5.71×10^{-5} for the two variants of GABMM. These results clearly demonstrate that PM offers superior accuracy while avoiding the limitations of the other approaches, namely restricted applicability (PSM) and high computational cost (GABMM).

Table 6: A comparison of the absolute errors for Example 7.8 with those reported in previous studies.

x	PM at $M = 10$	PSM [12] at $M = 10$, $\alpha_0 = \frac{3}{2}$	GABMM [9] at $M = 6$, $\alpha_0 = \frac{3}{2}$, $h = \frac{1}{20}$	GABMM [9] at $M = 6$, $\alpha_0 = \frac{3}{2}$, $h = \frac{1}{320}$
0.0	2.031×10^{-5}	—	—	—
0.1	1.650×10^{-5}	—	—	—
0.2	2.057×10^{-5}	—	—	—
0.3	1.835×10^{-5}	—	—	—
0.4	1.926×10^{-5}	—	—	—
0.5	1.524×10^{-5}	—	—	—
0.6	1.431×10^{-5}	—	—	—
0.7	9.560×10^{-6}	—	—	—
0.8	8.030×10^{-6}	—	—	—
0.9	2.920×10^{-6}	—	—	—
1.0	7.520×10^{-6}	6.83×10^{-4}	3.42×10^{-3}	5.71×10^{-5}

8. Conclusion

Based on the methodologies and numerical comparisons discussed, we conclude that the proposed operational matrices approach using shifted GPs effectively addresses two-point fractional-order boundary value problems involving Caputo derivatives. Our approach extends existing methods by incorporating fractional-order integral operational matrices in the Riemann-Liouville framework, allowing for the integration of monomial terms and transforming the problem into Sylvester-type matrix equations that can be solved. Unlike previous methods, our algorithm is versatile, handling polynomials as well as non-polynomial solutions efficiently. The numerical results show that the PM performs better than existing techniques such as the BCM, HWM, HPGF, PSM, GABMM, and FCFCD, especially in terms of computational efficiency and precision. Additionally, the effectiveness of our methodology, validated through extensive comparisons, highlights its potential for solving a wide range of fractional-order boundary value problems across various scientific and engineering applications. The proposed study is well-suited

for solving linear fractional-order initial and boundary value problems, providing a reliable and accurate numerical framework. However, the current algorithm is not directly applicable to nonlinear fractional-order problems involving either initial or boundary conditions. A natural extension of this work is to develop new operational matrices capable of handling nonlinearities, thereby broadening the scope of applicability to nonlinear FODEs. Moreover, the proposed methodology can be generalized to address fractional-order partial differential equations with both initial and boundary conditions, which often arise in modeling complex physical phenomena such as viscoelasticity, fluid flow, and anomalous diffusion.

From a computational perspective, future research may also integrate supervised machine learning techniques. In particular, GPs can be employed as activation functions in neural networks, with the weights between hidden and output layers trained using the Extreme Learning Machine algorithm. Such hybrid frameworks would open new directions for solving high-dimensional fractional models efficiently. Beyond theoretical advances, the methodology holds strong potential for practical applications in engineering, physics, and biological systems, where fractional-order models have demonstrated superior accuracy in capturing memory and hereditary effects. By bridging numerical analysis with machine learning, this line of research can contribute to the development of fast, reliable, and scalable tools for real-world problem solving.

Acknowledgment

The authors sincerely thank the anonymous reviewers for their valuable suggestions and constructive feedback, which have significantly improved the quality of this manuscript.

References

[1] V. Aboites, M. Ramírez, *Simple approach to special polynomials: Laguerre, Hermite, Legendre, Tchebycheff, and Gegenbauer*, In: Applied Mathematics, IntechOpen, London, (2019). 3

[2] R. B. Albadarneh, I. M. Batiha, M. Zurigat, *Numerical solutions for linear fractional differential equations of order $1 < \alpha < 2$ using finite difference method (FFDM)*, J. Math. Comput. Sci., **16** (2016), 103–111. 1

[3] Q. M. Al-Mdallal, M. I. Syam, M. N. Anwar, *A collocation-shooting method for solving fractional boundary value problems*, Commun. Nonlinear Sci. Numer. Simul., **15** (2010), 3814–3822. 7.1

[4] A. A. Al-Nana, I. M. Batiha, S. Momani, *A numerical approach for dealing with fractional boundary value problems*, Mathematics, **11** (2023), 12 pages. 1, 7.7, 7, 5

[5] T. J. Anastasio, *The fractional-order dynamics of brainstem vestibulo-oculomotor neurons*, Biol. Cybern., **72** (1994), 69–79. 1

[6] T. J. Anastasio, *Nonuniformity in the linear network model of the oculomotor integrator produces approximately fractional-order dynamics and more realistic neuron behavior*, Biol. Cybern., **79** (1998), 377–391. 1

[7] A. H. Bhrawy, T. M. Taha, *An operational matrix of fractional integration of the Laguerre polynomials and its application on a semi-infinite interval*, Math. Sci., **6** (2012), 7 pages. 1, 1, 4.1

[8] A. Chowdhury, S. Tanveer, X. Wang, *Nonlinear Two-Point Boundary Value Problems: Applications to a Cholera Epidemic Model*, Proc. A., **476** (2020), 23 pages. 1

[9] K. Diethelm, N. J. Ford, A. D. Freed, *Detailed error analysis for a fractional Adams method*, Numer. Algorithms, **36** (2004), 31–52. 1, 7.8, 6

[10] A. A. El-Kalaawy, E. H. Doha, S. S. Ezz-Eldien, M. A. Abdelkawy, R. M. Hafez, A. Z. M. Amin, D. Baleanu, M. A. Zaky, *A computationally efficient method for a class of fractional variational and optimal control problems using fractional Gegenbauer functions*, Rom. Rep. Phys, **70** (2018), 22 pages. 4.1

[11] B. Endeshaw, *Finite difference method for boundary value problems in ordinary differential equations*, Math. Theory Model., **9** (2019), 17–27. 1

[12] S. Esmaeili, M. Shamsi, *A pseudo-spectral scheme for the approximate solution of a family of fractional differential equations*, Commun. Nonlinear Sci. Numer. Simul., **16** (2011), 3646–3654. 1, 7.8, 6

[13] B. Ghanbari, A. Atangana, *Some new edge detecting techniques based on fractional derivatives with non-local and non-singular kernels*, Adv. Differ. Equ., **2020** (2020), 19 pages. 1

[14] V. M. Guibout, D. J. Scheeres, *Solving Two-Point Boundary Value Problems Using Generating Functions: Theory and Applications to Astrodynamics*, Elsevier Astrodynamics Series, **1** (2006), 53–105. 1

[15] R. M. Hafez, Y. H. Youssri, *Shifted Gegenbauer-Gauss collocation method for solving fractional neutral functional-differential equations with proportional delays*, Kragujevac J. Math., **46** (2022), 981–996. 4.1

[16] G. Infante, P. Pietramala, M. Tenuta, *Existence and localization of positive solutions for a nonlocal BVP arising in chemical reactor theory*, Commun. Nonlinear Sci. Numer. Simul., **19** (2014), 2245–2251. 1

[17] H. Jafari, S. Salati, M. Matinfar, V. T. Nguyen, *A numerical scheme for a class of nonlinear multi-order fractional differential equations*, Fractals, **33** (2025), 12 pages. 1
[18] T. Ji, J. Hou, C. Yang, *Numerical solution of the Bagley-Torvik equation using shifted Chebyshev operational matrix*, Adv. Differ. Equ., **2020** (2020), 14 pages. 1, 1, 4.1
[19] H. B. Keller, *Numerical Methods for Two-Point Boundary-Value Problems*, Dover Publications, Inc., New York, (1992). 1
[20] S. Kumar, V. Gupta, J. F. Gómez-Aguilar, *An efficient operational matrix technique to solve the fractional order non-local boundary value problems*, J. Math. Chem., **60** (2022), 1463–1479. 1
[21] R. L. Magin, *Fractional Calculus in Bioengineering*, Crit. Rev. Biomed. Eng., **32** (2004), 104 pages. 1
[22] R. L. Magin, *Fractional calculus models of complex dynamics in biological tissues*, Comput. Math. Appl., **59** (2010), 1586–1593. 1
[23] F. Marcellán, W. Van Assche, *Orthogonal polynomials and special functions: computation and applications*, Springer-Verlag, Berlin, (2006). 3
[24] M. Mekideche, Y. Ferdi, *Edge detection optimization using fractional order calculus*, Int. Arab J. Inf. Technol., **16** (2019), 827–832. 1
[25] A. Pálfalvi, *Efficient solution of a vibration equation involving fractional derivatives*, Int. J. Non-Linear Mech., **45** (2010), 169–175. 7.4, 7.4
[26] I. Podlubny, *Fractional differential equations*, Academic Press, Inc., San Diego, CA, (1999). 2.1, 2
[27] A. Rontó, M. Rontó, *Successive approximation techniques in non-linear boundary value problems for ordinary differential equations*, Elsevier/North-Holland, Amsterdam, (2008), 441–592. 1
[28] E. M. Stein, G. Weiss, *Introduction to Fourier analysis on Euclidean spaces*, Princeton University Press, Princeton, NJ, (1971). 3
[29] G. Szegő, *Orthogonal Polynomials*, American Mathematical Society, Providence, RI, (1975). 3
[30] I. Talib, M. N. Alam, D. Baleanu, D. Zaidi, *A decomposition algorithm coupled with operational matrices approach with applications to fractional differential equations*, Thermal Sci., **25** (2021), 449–455. 1, 1, 4.1
[31] I. Talib, M. Bohner, *Numerical study of generalized modified Caputo fractional differential equations*, Int. J. Comput. Math., **100** (2023), 153–176. 1, 1, 4.1
[32] P. J. Torvik, R. L. Bagley, *On the appearance of the fractional derivative in the behavior of real materials*, J. Appl. Mech., **51** (1984), 294–298. 7.3
[33] M. ur Rehman, R. A. Khan, *A numerical method for solving boundary value problems for fractional differential equations*, Appl. Math. Model., **36** (2012), 894–907. 1, 7.3, 2, 7, 7.4, 7.4, 3, 7.5, 4, 7.6
[34] M. Usman, M. Hamid, T. Zubair, R. U. Haq, W. Wang, M. B. Liu, *Novel operational matrices-based method for solving fractional-order delay differential equations via shifted Gegenbauer polynomials*, Appl. Math. Comput., **372** (2020), 17 pages. 3
[35] Y.-G. Wang, H.-F. Song, D. Li, *Solving two-point boundary value problems using combined homotopy perturbation method and Green's function method*, Appl. Math. Comput., **212** (2009), 366–376. 1, 7.5, 4, 7.6
[36] Ş. Yüzbaşı, *Numerical solution of the Bagley-Torvik equation by the Bessel collocation method*, Math. Methods Appl. Sci., **36** (2013), 300–312. 1, 7.2, 7, 1, 7.3, 2, 7
[37] M. Zaboli, H. Tajadodi, *A spectral collocation method for solving stochastic fractional integro-differential equation*, Math. Comput. Sci., **6** (2025), 1–31. 1
[38] D. Zaidi, I. Talib, M. B. Riaz, P. Agarwal, *Novel derivative operational matrix in Caputo sense with applications*, J. Taibah Univ. Sci., **18** (2024). 1, 1, 4.1